Journal Name

RSCPublishing

COMMUNICATION

Crystal-Facet-Dependent Hot-Electron Transfer in Plasmonic-Au/Semiconductor Heterostructures for Efficient Solar Photocatalysis

Cite this: DOI: 10.1039/x0xx00000x

Received 00th January 2012,
Accepted 00th January 2012

DOI: 10.1039/x0xx00000x

www.rsc.org/

Guigao Liu,[ab] Tao Wang,[b] Wei Zhou,[c] Xianguang Meng,[ab] Huabin Zhang,[b] Huimin Liu,[b] Tetsuya Kako,[b] and Jinhua Ye[abd]

Here, using Au-BiOCl as models, we show the significant crystal facet effects of semiconductor on hot-electron transfer within such plasmonic heterostructures under visible-light. It is found that {010} facets of BiOCl are greatly advantageous over {001} facets for the hot-electron injection, as evidenced by steady-state diffuse reflectance spectroscopy and photoelectrochemical measurements. Consequently, Au-BiOCl-010 exhibits a superior activity for photocatalytic aerobic oxidation of 2-propanol with a quantum efficiency of 1.3%, being 3.5 times higher than that of Au-BiOCl-001. The differences in band structure between {001} and {010} facets of BiOCl may account for the facet-dependent hot-electron transfer characteristics.

Semiconductor photocatalysis has received increasing attention for the direct utilization of solar energy in environmental remediation, water splitting for hydrogen or oxygen generation, and organic photosynthesis.[1] Although various semiconductor photocatalysts have been explored, some of the major constraints still involve in this process, such as low photocatalytic efficiency and limited visible-light photoabsorption.[2] It was discovered that the incorporation of plasmonic Au or Ag nanoparticles (NPs) onto semiconductors (*e.g.* TiO_2) has shown to greatly increase their photocatalytic activity with concomitant reaction rate enhancement in visible light region by using the surface plasmon resonance (SPR) of such metal NPs.[3] SPR can be described as the resonant photon-induced collective oscillation of surface electrons on metal NPs, simultaneously producing highly energetic hot electrons through non-radiative excitation.[3h] When the plasmonic-metal NPs are in contact with a semiconductor, the hot electrons can be directly injected into the conduction band (CB) of the semiconductor over the Schottky barrier, which offers the intrinsic driving force for the visible-light photocatalysis in these heterostructures.[3i]

Obviously, the plasmonic photocatalysts generally consist of two counterparts, *i.e.* the plasmonic metal particles and the semiconductors. During the past decades, the function of the plasmonic metal particles dependent on the shapes or sizes has been a topic of intense investigation because of their critical roles as visible-light harvesting antennas and electron or energy transfers in such composite photocatalysts,[3a, 3b, 3g, 3h] whereas, by contrast, semiconductor part (the hot electron acceptor) has received much less attention. Until recently, the significance of the structural and electronic properties of semiconductor materials on the photocatalytic activity for plasmonic catalysts was preliminary recognized by some researchers.[3e, 3f] For instance, Shiraishi *et al.* reported that the anatase/rutile interfaces in P25 TiO_2 could endow the Au NPs located more active for aerobic oxidation under visible-light irradiation due to the formation of the joint configuration consisting of Au/rutile/anatase phases which facilitated smooth electron transfer from the photoactivated Au particles to rutile and then to adjacent anatase.[3f] Majima *et al.* found that, compared with TiO_2 NPs, more hot electrons injected from the excited Au NPs could be accumulated in mesocrystal TiO_2 within a much shorter time and that they exhibited longer lifetime, thereby significantly improving the Au-SPR-induced photocatalytic activity.[3e] A recent report from our group also showed that the local electric nearfields resulted from the SPR excitation of Au nanocages could be dramatically increased by the non-centrosymmetric coupling with TiO_2 assemblies.[3a] These studies provide evidences for the essential role of semiconductor support in plasmonic photocatalysts and, more importantly, imply that more efforts should be dedicated in the modification of semiconductor for exploring more active plasmonic photocatalysts.

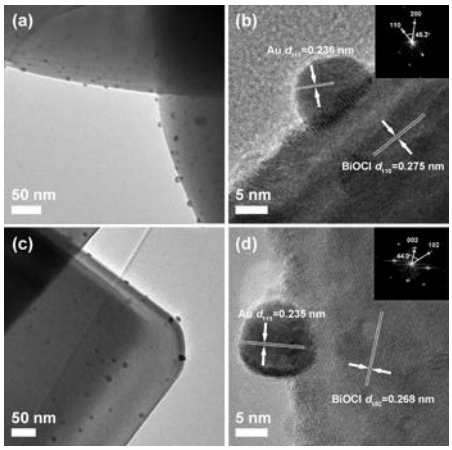

Figure 1. TEM and HR-TEM images of (a, b) BiOCl-001-Au and (c, d) BiOCl-010-Au. The insets in (b) and (d) are the Fast Fourier transform (FFT) patterns of BiOCl regions, further confirming the synthesis of BiOCl nanosheets with exposed {001} and {010} facets.

As mentioned above, hot-electron transfer from metal particles to neighbouring semiconductor upon visible-light excitation (simultaneously, leaving energetic holes on metal particles) drives the photocatalysis proceeding in plasmonic photocatalysts and consequently determines the solar energy conversion for such photocatalytic systems. However, this process remains a challenge because hot electrons suffer from rapid energy decay (on a femtosecond timescale) and meanwhile have to overcome relatively large Schottky barrier energy to reach the semiconductor.[3h, 3i, 4] Hence, a further understanding and exploration for hot-electron transfer within plasmonic photocatalysts is highly desirable, which might be of significance for providing guidance towards the alleviation of these issues and help to design and develop efficient SPR-induced visible-light photocatalysis. Recent investigations on crystal facet engineering of semiconductors have demonstrated theoretically and experimentally that photogenerated charge transfer on distinct crystal facets is closely related to their corresponding geometric and electronic properties.[5] Certain facets of a semiconductor may prefer the accumulation and transfer of photoexcited electrons, while others do not. For example, it was reported that, under visible-light irradiation, photogenerated electrons selectively travel to the {010} facets of $BiVO_4$ evidenced by the deposition of reduction cocatalysts, while oxidation reactions took place on the {110} facets.[5c] Although crystal-facet-dependent (photogenerated) electron transfer is well known in pure semiconductor photocatalysts, how the semiconductor-facet affects the hot-electron transfer in plasmonic photocatalysts is still ambiguous. In this work, we were encouraged to answer this question. Au NPs were deposited on BiOCl single-crystalline nanosheets with exposed {001} and {010} facets, respectively, to construct two kinds of semiconductor-facet-distinguishable plasmonic photocatalysts. We observed that photoexcited hot-electron transfers from Au NPs to BiOCl nanosheets were highly dependent on the electronic and structural properties of the exposed facets of semiconductors, consequently resulting in their facet-dependent photoreactivities. Apart from shedding light on the deep understanding of hot-electron transfer in SPR-induced photocatalysis, this finding can be exploited for rationally engineering more efficient plasmonic photocatalysts with potential applications in solar energy conversion.

BiOCl crystallizes in the layered tetragonal matlockite structure characterized by $[Bi_2O_2]$ slabs interleaved with double halogen atom slabs along the [001] direction (JCPDS 06-0249, $a = b = 3.89$ Å, $c = 7.37$ Å).[6] Here, BiOCl nanosheets with exposed {001} and {010} facets (denoted as BiOCl-001 and BiOCl-010, respectively) were selectively prepared via a reported hydrothermal method.[7] They were intentionally chosen as the Au nanoparticle support models because of their intrinsic surfactant-free surfaces and UV-light responsive characteristics, which ensured direct interfacial contact between Au NPs and semiconductor and meanwhile enabled us to independently investigate Au SPR-induced hot-electron transfer. Scanning electron microscopy (SEM) observation showed that BiOCl-001 consisted of relatively large-size sheets with widths of 1−4 μm and thicknesses of 90−300 nm (Figure S1a). Consistent with Zhang's report, these BiOCl nanosheets were enclosed by two {001} facets (bottom and top surfaces) and four {110} facets (lateral surfaces) (Figure S3a and Figure 1b).[7] Thus, the percentage of exposed {001} facets in BiOCl-001 was estimated to be ca. 77% through the geometric calculation. Also, the BiOCl-010 sample showed sheet-shape structures enclosed dominantly by {010} facets (Figure S3b and Figure 1d). The corresponding percentage of {010} facets was calculated to be ca. 82%. Au NPs were deposited on the BiOCl nanosheets (denoted as BiOCl-001-Au and BiOCl-010-Au) through the conventional deposition-precipitation strategy.[8] SEM and transmission electron microscopy (TEM) images (Figure S1b,d and Figure 1) showed that Au NPs are well-dispersed on the {001} and {010} facets of BiOCl nanosheets for BiOCl-001-Au and BiOCl-010-Au samples, respectively, with average diameters of 7.1 and 7.9 nm (Figure S2). High-resolution TEM (HR-TEM) revealed the highly crystalline nature of both BiOCl-001 and BiOCl-010 nanosheets, as well as the close interfacial contact between Au NPs and semiconductors. Specially, the lattice fringe spacings of 0.236, 0.275, and 0.275 nm are assigned to (111) of Au, (110) of BiOCl-001, and (102) of BiOCl-010, respectively. The loading amounts of Au were measured to be 1.3 at.% for BiOCl-001-Au and 1.0 at.% for BiOCl-010-Au by X-ray photoelectron spectroscopy (XPS) (Figure S5). The UV-vis diffuse reflectance spectra showed that BiOCl-001-Au and BiOCl-010-Au exhibited similar Au-SPR induced

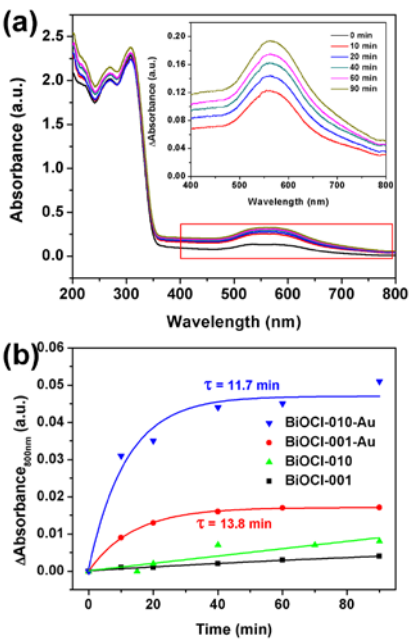

Figure 2. (a) UV-vis absorption spectra of BiOCl-010-Au in Ar-saturated methanol during visible-light irradiation. Differential spectra are drawn in the inset. (b) Time evolution of absorbance measured at 800 nm wavelength for different samples under visible-light irradiation.

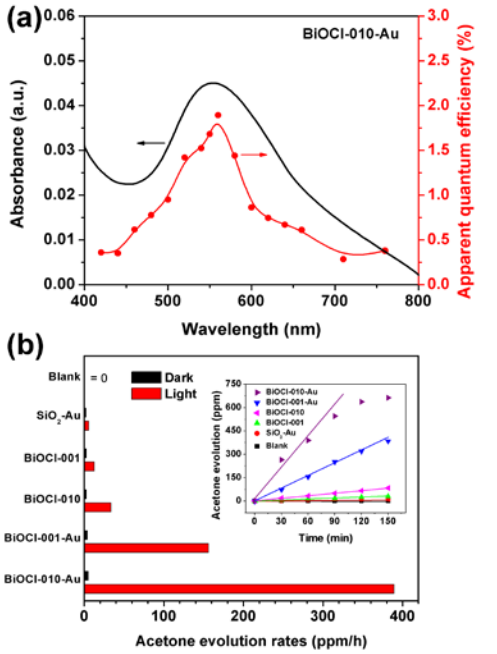

Figure 3. (a) Apparent quantum efficiencies for photocatalytic IPA oxidation over BiOCl-010-Au at various light wavelength ranges (The red curve are the trendlines added to guide the eye), consistent with its UV-visible absorption spectrum in air (black curve). (b) Rates of acetone evolution over various catalysts in the dark or under visible-light irradiation ($420 < \lambda < 800$ nm) (Blank indicates no catalysts). Inset shows the acetone evolution as a function of irradiation time (Since the IPA is not sufficient to saturate the surface, the acetone evolution rate over BiOCl-010-Au is shown to be obviously decreased after reacting for 90 min.).

photoabsorptions in visible-light range with peaks centered at ~580 nm (Figure S6). These data well demonstrate the successful preparation of two different BiOCl-Au plasmonic photocatalysts with Au NPs deposited on the {001} and {010} facets of BiOCl nanosheets, respectively.

Similar to TiO_2, BiOCl has no visible-light response but reduced BiOCl can absorb both visible-light and near-infrared light due to the formation of oxygen vacancies.[9] This phenomenon allows us to examine hot-electron transfer in the present plasmonic photocatalysts easily by steady-state diffuse reflectance spectroscopy.[3e, 9g] In the test, the sample was immersed in Ar-saturated methanol (methanol acts as scavenger for holes and the O_2-free environment guarantees that the injected hot electrons can be used to reduce BiOCl rather than O_2) and the steady-state diffuse reflectance spectra were recorded before and after visible-light irradiation. As shown in Figure 2a, with the irradiation time prolonged, the absorbance of BiOCl-010-Au in 400 to 800 nm wavelength range was clearly enhanced, suggesting the accumulation of hot electrons in BiOCl-010 nanosheets.[3e, 9e, 9g] Similar phenomenon was also observed for BiOCl-001-Au (Figure 2b and Figure S7). In contrast, the samples without Au loading (both BiOCl-001 and BiOCl-010) showed negligible visible-light absorption before and after constant irradiation. From a single-exponential fitting,[3e] the time constant of BiOCl-010-Au for absorption growth is estimated to be 11.7 min, which is smaller than that of BiOCl-001-Au of 13.8 min. Moreover, the concentration of stored hot electrons in BiOCl-010-Au corresponding to the absorption variation is much higher than that in BiOCl-001-Au. These results indicate that, compared with BiOCl-001, hot electrons from plasmonic Au NPs prefer to be injected and accumulated in BiOCl-010, presenting an interesting semiconductor-facet dependent hot-electron transfer characteristics.

To provide more evidences for this semiconductor-facet induced preferential transfer of hot electrons, a suite of photoelectrochemical (PEC) experiments were then performed. Electrochemical impedance spectroscopy (EIS) is a powerful tool to investigate the photogenerated carrier transfer and separation inside the electrode.[4b, 10] Accordingly, the representative EIS Nyquist plots for BiOCl-001-Au and BiOCl-010-Au are recorded in the range 0.01 Hz to 100 kHz using a three-electrode system. As shown in Figure S8, BiOCl-001-Au and BiOCl-010-Au present nearly equal dark charge transfer resistances. When upon visible-light illumination, clear decreases in resistance are observed in both two electrodes as a consequence of the fact that visible-light induces hot electron injection via optically exciting Au NPs.[4b] More importantly, the increased conductance in BiOCl-010-Au is significantly higher than that in BiOCl-001-Au, which is an additional reflection for more effective hot-electron transfer between Au and BiOCl-010. The consistent conclusion is also supported by photochronoamperometry measurements for the two electrode system in a 2-propanol contained electrolyte solution (Figure S9).[3d] Expectedly, visible-light irradiation leads to an anodic current when BiOCl-010-Au used as working electrode (WE) and BiOCl-001-Au as counter electrode (CE). On exchanging the electrodes (BiOCl-010-Au for CE and BiOCl-001-Au for WE), a cathodic photocurrent is exhibited. These results strongly suggest the net electron transfer from BiOCl-010-Au to BiOCl-001-Au, implying a higher transfer efficiency of hot electrons in BiOCl-010-Au by the SPR excitation.

The information of hot-electron transfer in plasmonic photocatalysts gleaned above has validated its semiconductor-facet-dependent characteristic. A proof-of-concept demonstration is further offered by using photocatalytic aerobic oxidation of 2-propanol (IPA) to acetone as a model reaction (please consult the Supporting Information for detailed discussion of SPR-induced aerobic oxidation mechanism, Scheme S1).[3a, 3b, 3d, 3f] The wavelength dependence of apparent quantum efficiency (AQE) for photocatalytic IPA oxidation over BiOCl-010-Au was first measured to distinguish if the activity is due to the SPR excitation of Au NPs or not. As shown in Figure 3a, the AQE depends strongly on the light source wavelength and it qualitatively tracks the characteristic plasmonic absorption of Au NPs.[11] This suggests that the IPA photo-oxidation is mainly induced by Au SPR excitation. The AQE at 560 ± 14 nm of BiOCl-010-Au reaches as high as 1.9%, which is comparable with that of the well-developed TiO_2-Au plasmonic photocatalysts.[3f] Figure 3b compares evolutions of acetone over different catalysts under visible-light irradiation (The effects of Au loading amounts and Au particle sizes on the activity are discussed in Figure S10). The BiOCl-010-Au turns out to have a high visible-light activity, much greater than the BiOCl-001-Au as expected. Precisely, the QE is calculated and a value of 1.3% is achieved by BiOCl-010-Au, which is 3.5 times that of BiOCl-001-Au (0.37%). Control experiments performed in the dark or irradiating SiO_2-Au catalysts lead to negligible acetone evolution, implying that the thermal catalytic effect of Au NPs on the oxidation is negligible. The activity of the catalysts for photocatalytic oxygen production from water was also evaluated and the BiOCl-010-Au still performed much better than BiOCl-001-Au (Figure S11), further supporting the above conclusion on facet-dependent hot-electron transfer even though it may involve an Au interband transition mechanism as detailedly discussed in our previous report.[13] Therefore, as discussed above, the superior visible-light activity of BiOCl-010-Au than BiOCl-001-Au supports that the {010} facet of BiOCl are

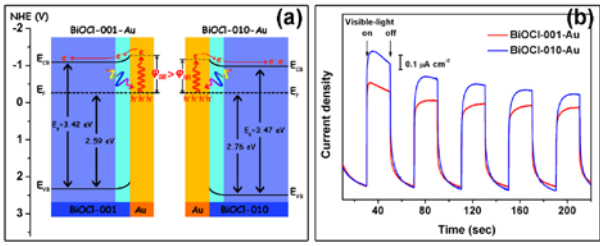

Figure 4. (a) Schematic band structures of BiOCl-001-Au and BiOCl-010-Au, showing the proposed hot-electron transfer from SPR-excited Au NPs to BiOCl by overcoming the corresponding Schottky barriers. (b) Photocurrent responses of BiOCl-001-Au and BiOCl-010-Au at an applied potential of 0.8 V vs. Ag/AgCl in 0.5 M Na_2SO_4 aqueous solutions under visible-light irradiation ($\lambda > 420$ nm).

significantly advantageous over the {001} facet for hot electron injection and transfer.

To elucidate the origin for the semiconductor-facet-dependent hot-electron transfer in the present plasmonic photocatalysts, their band structures are first carefully investigated. UV-vis absorption spectra of BiOCl-001 and BiOCl-010 give their band-gap energies of 3.42 and 3.47 eV, respectively (Figure S12). The relative positions of their valence bands (VB) to Fermi level (E_F) are also measured by VB-XPS (Figure S13). Electrochemical Mott–Schottky plots demonstrate their n-type character (Figure S14).[14] Hence, the obtained flat band potentials in conjunction with their VB positions and band-gap energies provide the band structures of BiOCl-001 and BiOCl-010 (Figure S15). After contact to form a Schottky junction between Au and BiOCl, alignment of their Fermi levels will occur and will be equilibrated again under irradiation, producing a potential barrier φ_{SB}.[3i, 4b, 12, 15] We assume that the aligned E_F in BiOCl-Au after equilibration is located at the original E_F of BiOCl and that the band bendings are identical for BiOCl-010-Au and BiOCl-001-Au. The band structures of BiOCl-Au can be illustrated as shown in Figure 4a. Under light illumination, the excitation of SPR in Au NPs transiently produces hot-electron/hole pairs. However, only the hot electrons with energies higher than the Schottky barrier energy φ_{SB} can be injected into the CB of BiOCl.[3i] Due to the much less negative CB level in BiOCl-010 than in BiOCl-001, a relative higher Schottky barrier is presented in BiOCl-001-Au. Therefore, it is understandable that the combination of BiOCl-010 nanosheets and Au NPs can potentially achieve more efficient hot-electron injection. An agreed conclusion is also obtained by theoretical calculation, which shows that the {010} facets in BiOCl significantly favor accumulating electrons over the {001} facets (See Supporting Information for a detailed discussion, Figure S16 and S17). Hence, given the fact of similar Au loadings, distributions and contact states on BiOCl between BiOCl-001-Au and BiOCl-010-Au (Figure 1 and Figure S5), the band structure properties might account for the semiconductor-facet dependent hot-electron transfer in these plasmonic photocatalysts, as further confirmed by the transient photocurrent measurements shown in Figure 4b. Both samples exhibit prompt and reproducible photocurrent responses to ON/OFF visible-light illumination cycles, but the photocurrent by BiOCl-010-Au is much higher than that by BiOCl-001-Au. This is indicative of more efficient hot-electron transfer in BiOCl-010-Au, well agreed with the discussion above.

Conclusions

In summary, BiOCl nanosheets with exposed {001} and {010} facets were selectively prepared and further modified with Au NPs to construct plasmonic photocatalysts (BiOCl-001-Au and BiOCl-010-Au). Taking these two photocatalysts as models, a semiconductor-facet dependent hot-electron transfer (from Au NPs to semiconductor and subsequently on semiconductor) is carefully confirmed, which is a result of the differences in band structures between BiOCl-001-Au and BiOCl-010-Au. Because of more efficient hot-electron transfer in BiOCl-010-Au, it exhibits a very high visible-light activity for aerobic oxidation of 2-propanol, much greater than that of BiOCl-001-Au. The findings from this study should be promising and intriguing for deeply understanding the hot-electron transfer in plasmonic photocatalysts, and designing highly efficient plasmonic photocatalysts for solar energy conversion applications.

This work received financial support from the World Premier International Research Center Initiative (WPI Initiative) on Materials Nanoarchitectonics (MANA), MEXT (Japan), and the National Basic Research Program of China (973 Program, 2014CB239301). G. Liu is grateful to Dr. S. Ouyang for his assistance in the writing of this manuscript.

Notes and references

[a] Graduate School of Chemical Science and Engineering, Hokkaido University, Sapporo, Japan. E-mail: Jinhua.YE@nims.go.jp

[b] Environmental Remediation Materials Unit and International Center for Materials Nanoarchitectonics (WPI-MANA), National Institute for Materials Science (NIMS), Tsukuba, Ibaraki, Japan.

[c] Department of Applied Physics, Tianjin Key Laboratory of Low Dimensional Materials Physics and Preparing Technology, Faculty of Science, Tianjin University, Tianjin, China.

[d] TU-NIMS Joint Research Center, School of Material Science and Engineering, Tianjin University, Tianjin, China.

† Electronic Supplementary Information (ESI) available: See DOI: 10.1039/c000000x/

(1) (a) X. Chen, S. Shen, L. Guo, S. S. Mao, *Chem. Rev.* **2010**, *110*, 6503; (b) M. R. Hoffmann, S. T. Martin, W. Choi, D. W. Bahnemann, *Chem. Rev.* **1995**, *95*, 69.
(2) H. Tong, S. Ouyang, Y. Bi, N. Umezawa, M. Oshikiri, J. Ye, *Adv. Mater.* **2012**, *24*, 229.
(3) (a) L. Liu, T. D. Dao, R. Kodiyath, Q. Kang, H. Abe, T. Nagao, J. Ye, *Adv. Funct. Mater.* **2014**, *24*, 7754; (b) L. Liu, S. Ouyang, J. Ye, *Angew Chem Int Ed* **2013**, *52*, 6689; (c) J. S. DuChene, B. C. Sweeny, A. C. Johnston-Peck, D. Su, E. A. Stach, W. D. Wei, *Angew. Chem. Int. Ed.* **2014**, *53*, 7887; (d) S.-i. Naya, T. Niwa, T. Kume, H. Tada, *Angew. Chem. Int. Ed.* **2014**, *53*, 7305; (e) Z. Bian, T. Tachikawa, P. Zhang, M. Fujitsuka, T. Majima, *J. Am. Chem. Soc.* **2013**, *136*, 458; (f) D. Tsukamoto, Y. Shiraishi, Y. Sugano, S. Ichikawa, S. Tanaka, T. Hirai, *J. Am. Chem. Soc.* **2012**, *134*, 6309; (g) K. Qian, B. C. Sweeny, A. C. Johnston-Peck, W. Niu, J. O. Graham, J. S. DuChene, J. Qiu, Y.-C. Wang, M. H. Engelhard, D. Su, E. A. Stach, W. D. Wei, *J. Am. Chem. Soc.* **2014**, *136*, 9842; (h) S. Linic, P. Christopher, D. B. Ingram, *Nat Mater* **2011**, *10*, 911; (i) C. Clavero, *Nat Photon* **2014**, *8*, 95.
(4) (a) K. Wu, W. E. Rodríguez-Córdoba, Y. Yang, T. Lian, *Nano Lett.* **2013**, *13*, 5255; (b) S. Mubeen, G. Hernandez-Sosa, D. Moses, J. Lee, M. Moskovits, *Nano Lett.* **2011**, *11*, 5548.
(5) (a) N. Roy, Y. Sohn, D. Pradhan, *ACS Nano* **2013**, *7*, 2532; (b) J. Yu, J. Low, W. Xiao, P. Zhou, M. Jaroniec, *J. Am. Chem. Soc.* **2014**, *136*, 8839; (c) R. Li, F. Zhang, D. Wang, J. Yang, M. Li, J. Zhu, X. Zhou, H. Han, C. Li, *Nat Commun* **2013**, *4*, 1432; (d) T. Tachikawa, N. Wang , S. Yamashita, S.-C. Cui, T. Majima, *Angew. Chem. Int. Ed.* **2010**, *49*, 8593; (e) L. Wang, J. Ge, A. Wang, M. Deng, X. Wang, S. Bai, R. Li, J. Jiang, Q. Zhang, Y. Luo, Y. Xiong, *Angew. Chem. Int. Ed.* **2014**, *53*, 5107. (f) C.-S. Tan, S.-C. Hsu, W.-H. Ke, L.-J. Chen, M. H. Huang, *Nano Lett.* **2015**, *15*, 2155. (g) M. H. Huang, S. Rej, S.-C. Hsu, *Chem. Commun.* **2014**, *50*, 1634.
(6) H. Cheng, B. Huang, Y. Dai, *Nanoscale* **2014**, *6*, 2009.
(7) J. Jiang, K. Zhao, X. Xiao, L. Zhang, *J. Am. Chem. Soc.* **2012**, *134*, 4473.

(8) C. Gomes Silva, R. Juárez, T. Marino, R. Molinari, H. García, *J. Am. Chem. Soc*. **2010**, *133*, 595.
(9) (a) Y. H. Hu, *Angew. Chem. Int. Ed*. **2012**, *51*, 12410; (b) C. Mao, F. Zuo, Y. Hou, X. Bu, P. Feng, *Angew. Chem. Int. Ed.* **2014**, *53*, 10485; (c) Q. Kang, J. Cao, Y. Zhang, L. Liu, H. Xu, J. Ye, *J. Mater. Chem. A* **2013**, *1*, 5766; (d) G. Wang, H. Wang, Y. Ling, Y. Tang, X. Yang, R. C. Fitzmorris, C. Wang, J. Z. Zhang, Y. Li, *Nano Lett.* **2011**, *11*, 3026; (e) L. Ye, K. Deng, F. Xu, L. Tian, T. Peng, L. Zan, *Phys. Chem. Chem. Phys.* **2012**, *14*, 82; (f) Y. Yu, C. Cao, H. Liu, P. Li, F. Wei, Y. Jiang, W. Song, *J. Mater. Chem. A* **2014**, *2*, 1677; (g) T. Tachikawa, S. Tojo, M. Fujitsuka, T. Sekino, T. Majima, *J. Phys. Chem. B* **2006**, *110*, 14055.
(10) (a) J. Hou, C. Yang, H. Cheng, S. Jiao, O. Takeda, H. Zhu, *Energy Environ. Sci.* **2014**, *7*, 3758; (b) F. Su, T. Wang, R. Lv, J. Zhang, P. Zhang, J. Lu, J. Gong, *Nanoscale* **2013**, *5*, 9001; (c) S. A. Ansari, M. M. Khan, M. O. Ansari, J. Lee, M. H. Cho, *J. Phys. Chem. C* **2013**, *117*, 27023; (d) X. Mou, B. Zhang, Y. Li, L. Yao, X. Wei, D. S. Su, W. Shen, *Angew. Chem. Int. Ed*. **2012**, *51*, 2989; (e) Y. Hou, F. Zuo, A. P. Dagg, J. Liu, P. Feng, *Adv. Mater*. **2014**, *26*, 5043.
(11) D. B. Ingram, S. Linic, *J. Am. Chem. Soc*. **2011**, *133*, 5202.
(12) L. Liu, P. Li, A. Boonchun, S. Ouyang, N. Umezawa, J. Ye, R. Kodiyath, T. Tanabe, R. V. Gubbala, S. Ueda, H. Abe, *J. Mater. Chem. A* **2014**, *2*, 9875.
(13) L. Liu, P. Li, B. Adisak, S. Ouyang, N. Umezawa, J. Ye, R. Kodiyath, T. Tanabe, G. V. Ramesh, S. Ueda, H. Abe, *J. Mater. Chem. A* **2014**, *2*, 9875.
(14) Y. Shiraishi, S. Kanazawa, Y. Kofuji, H. Sakamoto, S. Ichikawa, S. Tanaka, T. Hirai, *Angew. Chem. Int. Ed.* **2014**, *53*, 13454.
(15) V. Subramanian, E. E. Wolf, P. V. Kamat, *J. Am. Chem. Soc.* **2004**, *126*, 4943.